Article

J. Mex. Chem. Soc. **2024**, *68*(2)
Regular Issue

ISSN-e 2594-0317

Non-covalent Interactions in Dihalogenated Compounds $Ch(C_6H_4CH_2X)_2$ (Ch = O, S; X = Cl, Br, I). Synthesis, Crystal Structure, and Hirshfeld Surface Analysis

J. Viridiana García-González, José G. Alvarado-Rodríguez*, Noemí Andrade-López, Cristian G. Guerra-Poot

Área Académica de Química, Universidad Autónoma del Estado de Hidalgo, km. 4.5 Carretera Pachuca-Tulancingo, Col. Carboneras. C.P. 42184.Mineral de la Reforma, Hidalgo, México.

***Corresponding author:** José G. Alvarado-Rodríguez, email: jgar@uaeh.edu.mx

Received March 29th, 2023; Accepted June 6th, 2023.

DOI: http://dx.doi.org/10.29356/jmcs.v68i2.2036

Abstract. In this work, the synthesis and structural study by means of single-crystal X-ray diffraction of compounds of general formula **Ch**$(C_6H_4CH_2$**X**$)_2$ (**Ch** = O, S; **X** = Cl, Br, I) is reported. These compounds contain two flexible hydrocarbonated arms –CH_2–**X** in the *ortho* positions to the **Ch** heteroatom. These compounds were synthesized through a linear synthesis starting from diphenylether or diphenylsulfide. Based on the structural analysis, we describe the more relevant molecular features as well as the non-covalent interactions that the heavy halogen atoms display with other moieties that promote the cohesion of the crystal arrangement. The Hirshfeld analysis displayed that the **X**···π, **X**···**X**, and C–H···**X** interactions are quite significant in the crystal arrangement.
Keywords: Non-covalent interactions; dihalogenated compounds; Hirshfeld surfaces.

Resumen. En este trabajo, se describen la síntesis y el estudio estructural de difracción de rayos-X de monocristal de seis compuestos con fórmula general **Ch**$(C_6H_4CH_2$**X**$)_2$ (**Ch** = O, S; **X** = Cl, Br, I), que contienen dos brazos hidrocarbonados flexibles –CH_2–**X** en las posiciones *orto* al heteroátomo **Ch**. Estos compuestos fueron sintetizados a través de una síntesis lineal, partiendo de difeniléter o difeniltioéter. A través del análisis estructural se describen las características moleculares más relevantes, así como las interacciones no-covalentes que presentan los átomos de halógeno pesados con otros grupos funcionales para dar cohesión a la red cristalina. El estudio de las superficies de Hirshfeld mostró que las interacciones **X**···π, **X**···**X** y C–H···**X** son muy relevantes en esta cohesión.
Palabras clave: Interacciones no-covalentes; compuestos dihalogenados; superficies de Hirshfeld.

Introduction

In many aspects, the physicochemical properties and reactivity of halogenated organic compounds is strongly based on the nature of the **X** halogen substituent (**X** = F, Cl, Br, or I); for example, with an increase in the atomic number of the halogen, C–X bond energies decrease markedly, i.e., C–F > C–Cl > C–Br > C–I [1], and the order of reactivity can generally be predicted by the relative easiness with which the respective carbon–halogen bonds are broken. Other features such as the electron-withdrawing effect, atomic size, and polarizability of the halogen substituent also affect the reactivity of these halogenated compounds [2]. A typical reaction of these compounds is nucleophilic substitution of the halogen by electron-rich molecules or anions

J. Mex. Chem. Soc. **2024**, *68*(2)
Regular Issue

ISSN-e 2594-0317

such as ammonia, cyanide (a pseudohalide), hydroxide, alkoxides, or even another halogen [3]. In this vein, halogen-by-halogen exchange substitution provides a convenient route for synthesizing alkyl halides [4]. Other typical and very useful reaction of alkyl halides involves the formation of free radicals in the presence of very active alkaline or alkaline earth metals; subsequent reaction of these radicals can lead to the formation of organometallic compounds or coupling of the alkyl radicals to enlarge carbon chains [5].

On the other hand, the presence of a halogen atom makes possible the formation of either **Y**–**X**···**A** intra- or intermolecular non-covalent interactions; here, **Y**–**X** is the halogen bond donor such as I_2, Br_2, ICl, haloalkanes; haloarenes, haloimides, etc., meanwhile **A** represents the halogen bond acceptor that can be an atom with an electronic lone pair, a p system, or an anion [6,7]. Moreover, the halogen atom usually displays two regions; an electrophilic region diametrically opposed to the **Y**–**X** sigma bond (named as a σ-hole) and a nucleophilic region transversal to the stated bond (Fig. 1). Hence, due to the anisotropic distribution of the electron density, these two interactions have an important electrostatic component. [8]

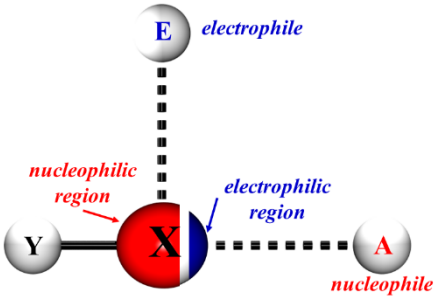

Fig. 1. Diagrammatic representation of an **X**···**A** halogen bond; also, is displayed a possible transversal **E**···**X** interaction.

A chief key to the formation halogen bonds is the polarizability of the halogen atom. Therefore, the strongest halogen bonds are formed by the most easily polarizable halogens, and the strength of the halogen bonds typically decreases in the order I > Br > Cl > F [9]. Several distinctive features of **X**···**A** halogen bond, such as the high directionality and strength tunability, prompted a plethora of applications in organocatalysis [10], crystal engineering [11]and drug design [12], and their influence on packing modes and the consequent orientation of organic molecules, are also considered important in conjunction with the practically ubiquitous both classical and no-classical hydrogen bond [13,14].

Thus, as a part of our studies in the reactivity of halogenated compounds [15], herein we report the structural analysis in crystalline state of two series of conformationally flexible di(2-halomethylphenyl)ethers (compounds **3a**, **4a**, and **5a**) and di(2-halomethylphenyl)thioethers (compounds **3b**, **4b**, and **5b**) of general formula **Ch**($C_6H_4CH_2$**X**)$_2$, where **Ch** is a chalcogen atom (oxygen or sulfur) and **X** = Cl, Br or I. To provide a structural context, in the 3D pie chart showed in Fig. 2 are presented the results of a delimited search in the Cambridge structural database for compounds containing at least one C_6–CH_2–**X** moiety.

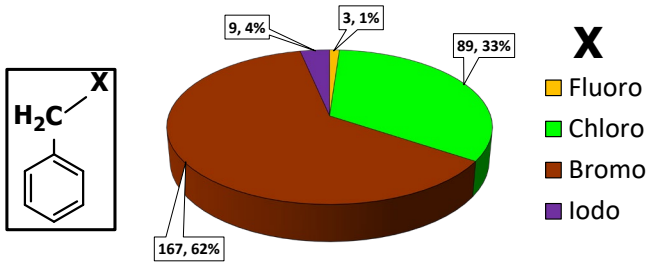

Fig. 2. Numerical and relative proportion of halocompounds containing at least one C_6–CH_2–**X** moiety. (268 hits; data retrieved from CSD version 5.43, updated to November 2022).

J. Mex. Chem. Soc. **2024**, *68*(2)
Regular Issue

ISSN-e 2594-0317

From these data, it is clear the dominance of the bromomethylenic compounds (167 compounds), and the scarceness of fluoro- and iodo- ones. In addition, we want to highlight two experimental facts: the first one is that the presence of two conformationally flexible –CH_2–**Br** arms in 1,4-dibromo-2,5-bis(bromomethyl)benzene allowed dimorphism, displaying Br···Br non-covalent interactions in solid crystalline state [16]. The second one is that there is just one compound with a slightly similar chemical environment to **3a-5a** and **3b-5b**, reported as a private communication (Ref. CSD code MUMQAO) [17].

In the title compounds, the presence of two –CH_2–**X** arms of different nature in both series prompted the formation of several **X**···p and **X**···**X** alongside to C–H···**X** interactions. A Hirshfeld surface analysis was carried out to describe the interactions present in the isostructural compounds.

Experimental

Instrumentation and software

Melting points were determined with a Mel–Temp II instrument. IR spectra were recorded in the 4,000–400 cm^{-1} range on a Perkin-Elmer System 2000 FT-IR spectrometer, as KBr pellets. ^1H and ^{13}C NMR spectra were recorded in $CDCl_3$ on a Bruker Avance III 400 MHz spectrometer (400.1 MHz for ^1H and 100.0 MHz for ^{13}C) at 23 °C and calibrated by using the residual proton resonance of $CDCl_3$. Chemical shifts (δ) are reported in ppm and coupling constants (*J*) are in Hz. For the assignment we used 2D correlation experiments such as COSY, HSQC and HMBC.

Suitable crystals for the X-ray diffraction analysis were obtained for compounds **3a**, **4a**, **5a**, **4b**, and **5b** by slow evaporation of CH_2Cl_2 solutions. Each single crystal was either glued on a tip of a thin glass fiber or mounted on a Nylon loop. Diffraction data were collected at 294 K in an Agilent Gemini diffractometer equipped with an Atlas CCD detector; we used graphite-monochromated Mo-Kα radiation (0.71073 Å). Absorption corrections were made by multi-scan methods using the CrysAlisPro software [18]. By using the Olex2 interface [19], the structures were solved by intrinsic phase methods using SHELXT [21] and all the non-hydrogen atoms were anisotropically refined by full-matrix least-squares on F^2 using SHELXL [22]. Hydrogen atoms were placed in their calculated positions and then refined using the riding model. Crystallographic data are listed in Table 1, and selected bond distances and angles are given in Table 2. The asymmetric unit of **3a** displayed just the half of the molecule (see gray moiety in Fig. 3); the other half is related by a two-fold axis, where the oxygen atom is placed on it (see green moiety in Fig. 3). The ORTEP views of the molecular structures are shown in Figures 3 and 4.

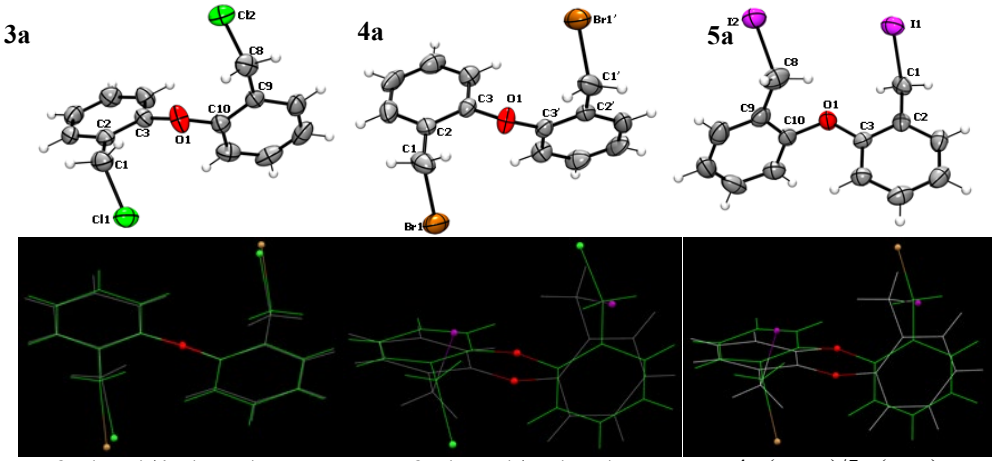

3a (gray)/**4a** (green) overlaying (RMSD = 0.154 Å; deviation$_{max}$ = 0.359 Å)

3a (green)/**5a** (gray) overlaying (RMSD = 1.172 Å; deviation$_{max}$ = 3.234 Å)

4a (green)/**5a** (gray) overlaying (RMSD = 1.281 Å; deviation$_{max}$ = 3.578 Å)

Fig. 3. Molecular structures of O($C_6H_4CH_2$**X**)$_2$ compounds (ORTEP at 50 %) and overlay results of the corresponding pairs.

J. Mex. Chem. Soc. **2024**, *68*(2)
Regular Issue

ISSN-e 2594-0317

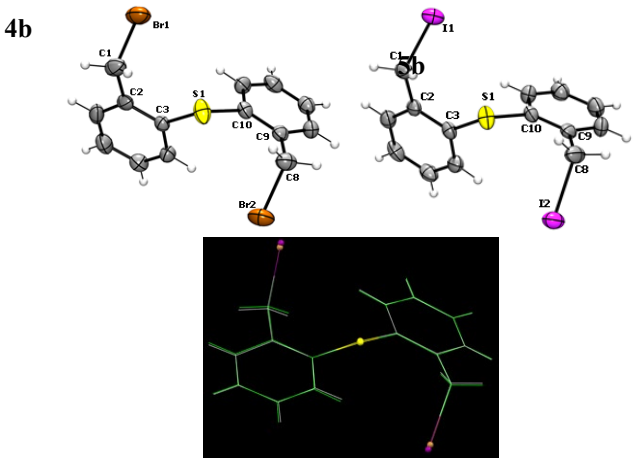

4b (gray)/**5b** (green) overlaying
(RMSD = 0.064 Å;
deviation$_{max}$ = 0.1544 Å)

Fig. 4. Molecular structures of $S(C_6H_4CH_2\mathbf{X})_2$ compounds (ORTEP at 50 %) and overlay results of the pair.

Table 1. Crystal data and refinement details.

	3a	**4a**	**5a**	**4b**	**5b**
Empirical formula	$C_{14}H_{12}Cl_2O$	$C_{14}H_{12}Br_2O$	$C_{14}H_{12}I_2O$	$C_{14}H_{12}Br_2S$	$C_{14}H_{12}I_2S$
Formula weight [g/mol]	267.14	356.06	450.04	372.12	466.10
Crystal system	triclinic	monoclinic	monoclinic	triclinic	triclinic
Space group	*P*–1	*I*2/a	$P2_1$	*P*–1	*P*–1
a [Å]	7.6808(4)	12.279(3)	8.2871(4)	8.2610(14)	8.2734(5)
b [Å]	7.9888(4)	9.2954(17)	4.6487(3)	9.2086(13)	9.5171(7)
c [Å]	10.7391(4)	11.972(3)	18.5371(12)	10.6912(17)	10.7511(9)
α [º]	87.075(4)	90	90	102.043(13)	103.115(7)
β [º]	79.474(4)	99.17(2)	90.603(5)	101.772(14)	101.149(6)
γ [º]	83.979(4)	90	90	113.586(15)	112.203(6)
V [Å^3]	643.95(5)	1349.1(5)	714.09(7)	690.4(2)	725.83(10)
Z	2	4	2	2	2
r_{calc} [g/cm^3]	1.378	1.753	2.093	1.790	2.133
Absorption coefficient [mm^{-1}]	0.484	5.990	4.386	5.996	4.453
F(000)	276	696.0	420.0	364.0	436.0

J. Mex. Chem. Soc. **2024**, *68*(2)
Regular Issue

ISSN-e 2594-0317

Crystal size [mm^3]	0.3 × 0.2 × 0.1	0.3 × 0.3 × 0.2	0.2 × 0.2 × 0.1	0.5 × 0.5 × 0.5	0.2 × 0.1 × 0.1
2Θ range data collection [º]	6.068 to 59.062	6.722 to 59.244	6.562 to 59.278	6.858 to 59.262	6.85 to 59.148
Measured reflections	23203	5234	18168	5913	5595
Data/restraints/parameters	3407/0/154	1678/0/78	3656/1/154	3262/0/154	3432/0/155
R_1; wR_2 [I>2□(I)]	0.0416, 0.0900	0.0442; 0.1146	0.0279; 0.0528	0.0458; 0.0795	0.0609; 0.0871
R_1; wR_2 [All data]	0.0680, 0.1026	0.0975; 0.1381	0.0417; 0.0578	0.1054; 0.1016	0.1339; 0.1079
Goodness-of-fit on F^2	1.031	1.040	1.039	0.995	1.031
Largest diff. peak / hole [$eÅ^{-3}$]	0.27/−0.30	0.63/−0.57	0.46/−0.52	0.33/−61	1.77/−1.32
Flack parameter	Not applicable	Not applicable	−0.019(16)	Not applicable	Not applicable
CCDC	2252394	2252390	2252392	2252393	2252391

Table 2. Selected bond lengths (Å) and angles (°) for **Ch**($C_6H_4CH_2$**X**)$_2$.

	3a	**4a**	**5a**	**4b**	**5b**
	(**Ch** = O **X** = Cl)	(**Ch** = O **X** = Br)	(**Ch** = O **X** = I)	(**Ch** = S **X** = Br)	(**Ch** = S **X** = I)
C–**X**	1.801(2); 1.802(2)	1.950(4)	2.180(6); 2.150(6)	1.971(4); 1.968(4)	2.170(5); 2.163(5)
C–**Ch**	1.383(2); 1.385(2)	1.381(4)	1.368(6); 1.408(6)	1.783(4); 1.794(3)	1.776(4); 1.769(4)
C–**Ch**–C	119.22(14)	118.5(4)	118.9(4)	101.03(17)	101.6(2)
C2–C3–**Ch**–C10	140.64(16)	138.6(4)	179.0(5)	134.9(3)	137.0(4)
C9–C10–**Ch**–C3	144.21(16)	138.6(4)	102.3(6)	127.3(3)	126.8(4)
$\|\Delta_{ta}\|$	3.57	0.0	76.7	7.6	10.2

$|\Delta_{ta}|$ is the difference of the C–C–**Ch**–C torsion angles; see text.

The atomic coordinates of all **3a**–**5a** diphenylether and **4b** and **5b** diphenylthioether compounds determined by X-ray crystallographic studies at 294 K were used to construct the molecular Hirshfeld surfaces based on the electron distribution calculated as the sum of spherical atomic electron densities (the promolecule), which dominates the corresponding sum over the crystal (the procrystal) yielding an implicit 0.5 value for the promolecule-to-procrystal ratio. The bond lengths involving hydrogen atoms were adjusted to values derived

J. Mex. Chem. Soc. **2024**, *68*(2)
Regular Issue

ISSN-e 2594-0317

from neutron diffraction [22]. The Hirshfeld surfaces mapped with d_{norm} and 2D fingerprint plots presented were generated using CrystalExplorer21 with a high standard surface resolution [23]. They were mapped using a fixed color scale, red-white-blue, where red highlights are for contacts shorter than van der Waals (vdW) radii sum, white for contacts around vdW separation, and blue is for contacts longer than the vdW sum.

The molecular electrostatic potential mapping (MEP) was calculated to characterize the close contacts by projecting the Hirshfeld surface with this MEP. We used the Tonto quantum modelling package [24] implemented in CrystalExplorer21 using the Becke three-parameter Lee–Yang–Parr (B3LYP) hybrid functionals [25] with the DGDZVP basis set [26,27].

General methods

All manipulations involving *n*-BuLi reagent were performed in a dry nitrogen atmosphere using standard Schlenk techniques. Solvents, *N,N,N′N′*-tetramethylethylenediamine (TMEDA), and *N,N*-dimethylformamide (DMF) were purchased from Sigma-Aldrich and dried by standard methods and distilled prior to use. The reagents used in the syntheses were purchased from Aldrich and used without purification. Merck Kiesel gel 60 (0.063–0.40 mm) was used for column chromatography.

The sequence of the reaction steps is summarized in Scheme 1. Dihalogenated compounds **3a**, **3b**, **4a**, **4b**, **5a** and **5b** were prepared by linear synthesis, starting from either diphenylether or diphenylthioether, respectively (the **a** letter refers to the compounds with **Ch** = oxygen and **b** to compounds with **Ch** = sulfur).

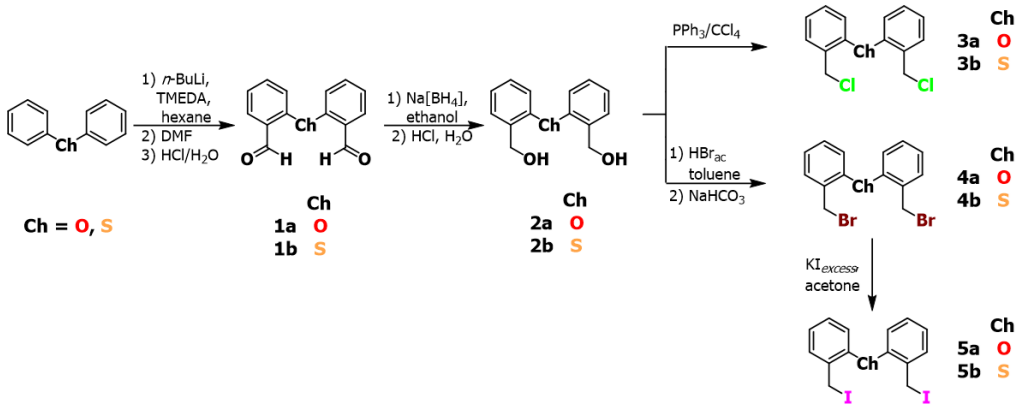

Scheme 1. Synthesis of dihalogenated compounds.

Synthesis of the dialdehyde $O(C_6H_4CHO)_2$ (1a)

Dialdehyde **1a** is known from the literature [28, 29]. Modification of this method allowed the desired product to be obtained in a much higher yield and without purification by column chromatography. Diphenylether (6.5 mL, 41 mmol) was dissolved in dry hexane (40 mL) under an inert nitrogen atmosphere, and TMEDA (13.5 mL, 90.2 mmol) was added at 25 °C. A solution of *n*-butyllithium in hexane (2.5 M, 36.1 mL, 90.2 mmol) was added dropwise to the stirred reaction mixture at 0 °C. This mixture was stirred at 0 °C for 22 h, turning into a beige one. Then, dry DMF (11.5 mL, 147.6 mmol) was poured dropwise into the reaction mixture. The white solution was stirred for 1 h at 70 °C. Aqueous hydrochloric acid (40 mL HCl in 60 mL of distilled water) was added, and the mixture was stirred for fifteen minutes. After, the compound was extracted with $CHCl_3$ (30 mL). The combined organic phases were dried with Na_2SO_4, and the volatiles were removed under reduced pressure to yield the title compound as a beige solid (8.8 g, 95 %).

mw = 226.22 g/mol. mp = 65 °C. IR (KBr, cm^{-1}): ν = 3071, 2856, 2755, 1685, 1599, 1472, 1455, 1394, 1276, 1224, 1097, 881, 827, 758. ^{1}H-RMN (400 MHz, $CDCl_3$, ppm) δ = 10.50 (s, 2H, H1), 7.99 (d, ^3J = 7.69 Hz, 2H, H7), 7.59 (t, ^3J = 7.69 Hz, 2H, H5), 7.30 (t, ^3J = 7.80 Hz, 2H, H6), 6.96 (d, ^3J = 8.32 Hz, 2H, H4). ^{13}C{^{1}H}-RMN (100 MHz, $CDCl_3$, ppm) δ = 188.7 (C1), 158.9 (C3), 136.1 (C5), 129.3 (C7), 127.3 (C2), 124.6 (C6), 119.2 (C4).

J. Mex. Chem. Soc. **2024**, *68*(2)
Regular Issue

ISSN-e 2594-0317

Synthesis of $O(C_6H_4CH_2OH)_2$ (2a)

The diol **2a** is known from the literature [30]; here is introduced an alternative procedure to obtain it in a much higher yield. Thus, to an ethanolic solution (60 mL) of **1a** (8.8 g, 38.9 mmol) was slowly added $Na[BH_4]$ (3.8 g, 97.4 mmol), and the resulting mixture was stirred for 1 h at 0 °C and three hours at room temperature. Then, it was acidified with diluted HCl (40 mL HCl in 60 mL of distilled water), followed by extraction with CH_2Cl_2 (60 mL). The combined organic phases were washed with brine (60 mL), dried (Na_2SO_4), and the volatiles were removed under reduced pressure. The product was obtained as a white solid (9.35 g, 99 %).

mw = 230.25 g/mol. mp = 86 °C. IR (KBr, cm^{-1}): ν = 3272 (OH), 3082, 3039, 2929, 2886, 1689, 1604, 1581, 1484, 1452, 1230, 1110, 1034, 880, 755. ^{1}H-RMN (400 MHz, $CDCl_3$, ppm) δ = 7.39 (d, ^3J = 7.19 Hz, 2H, H7), 7.25 (td, ^3J = 7.69 Hz, ^4J = 1.22 Hz, 2H, H5), 7.10 (td, ^3J = 7.44 Hz, ^4J = 0.69 Hz, 2H, H6), 6.82 (d, ^3J = 8.06 Hz, 2H, H4), 4.68 (s, 4H, H1). $^{13}C\{^1H\}$-RMN (100 MHz, $CDCl_3$, ppm) δ = 154.8 (C3), 131.4 (C7), 130.1 (C5), 129.3 (C2), 123.7 (C6), 117.9 (C4), 61.2 (C1).

Synthesis of the dichlorinated compound $[\{O(C_6H_4CH_2)_2\}Cl_2]$ (3a)

To a reaction flask, were added the diol **2a** (1.0 g, 4.3 mmol), carbon tetrachloride (20 mL), and triphenylphosphine (2.73 g, 10.4 mmol). The solution was heated at 65–70 °C for 24 h, and the reaction mixture was cooled and filtered. The yellow solution was chromatographed over a silica gel column with hexane/dichloromethane (1:1). The solution was evaporated to give a colorless crystalline solid (0.50 g, 43%).

mw = 267.14 g/mol. mp = 68 °C. IR (KBr, cm^{-1}): ν = 3036, 2922, 2851, 1581, 1483, 1452, 1239, 1193, 1104, 914, 748, 672. ^{1}H-RMN (400 MHz, $CDCl_3$, ppm) δ = 7.50 (dd, ^3J = 7.60 Hz, ^4J = 1.50 Hz, 2H, H7), 7.28 (td, ^3J = 7.60 Hz, ^4J = 1.5 Hz, 2H, H5), 7.14 (t, ^3J = 7.40 Hz, 2H, H6), 6.83 (d, ^3J = 8.00 Hz, 2H, H4), 4.73 (s, 4H, H1). $^{13}C\{^1H\}$-RMN (100 MHz, $CDCl_3$, ppm) δ = 154.9 (C3), 131.2 (C7), 130.3 (C5), 128.7 (C2), 124.1 (C6), 118.5 (C4), 41.2 (C1).

Synthesis of dibrominated compound $[\{O(C_6H_4CH_2)_2\}Br_2]$ (4a)

Dibrominated compound **4a** was synthesized according with the literature procedure [30]. To a toluene solution (30 mL) of **2a** (9.35 g, 40.6 mmol), was added dropwise HBr (15.3 mL, 142.1 mmol) dissolved in toluene (10 mL), and the resulting mixture was refluxed for 22 h. Then, saturated aqueous $NaHCO_3$ solution (20 mL) was carefully added, followed by extraction with CH_3Cl_3 (20 mL). The organic phase was separated, dried (Na_2SO_4), and evaporated to obtain a brown solid. The compound was purified by washing it with cold ethanol, to obtain a white crystalline solid (6.37 g, 44 %).

mw = 356.04 g/mol. mp = 92 °C. IR (KBr, cm^{-1}): ν = 3058, 3034, 2985, 1579, 1485, 1449, 1242, 1185, 899, 775, 605. ^{1}H-RMN (400 MHz, $CDCl_3$, ppm) δ = 7.49 (d, ^3J = 7.60 Hz, 2H, H7), 7.28 (t, ^3J = 8.00 Hz, 2H, H5), 7.13 (t, ^3J = 7.60 Hz, 2H, H6), 6.85 (d, ^3J = 9.20 Hz, 2H, H4), 4.66 (s, 4H, H1). $^{13}C\{^1H\}$-RMN (100 MHz, $CDCl_3$, ppm) δ = 154.9 (C3), 131.5 (C7), 130.3 (C5), 129.0 (C2), 124.1 (C6), 118.6 (C4), 28.2 (C1).

Synthesis of diiodo compound $[\{O(C_6H_4CH_2)_2\}I_2]$ (5a)

Preparation of **5a** was based on literature methods where the starting materials are also primary alcohols [31, 32]. Thus, KI (3.5 g, 21.0 mmol) was added to **4a** (3 g, 8.4 mmol) previously dissolved in acetone (40 mL). This mixture was refluxed for 22 h. Next, the solvent was removed in vacuo, and the residue was dispersed in CH_2Cl_2 (50 mL). The resulting precipitate was filtered off, and the solvent was removed in vacuo to yield **5a** as a brown solid (3.7 g, 97 %).

mw = 450.0 g/mol. mp = 96 °C. IR (KBr, cm^{-1}): ν = 3034, 2972, 1577, 1484, 1450, 1243, 1150, 894, 755. ^{1}H-RMN (400 MHz, $CDCl_3$, ppm) δ = 7.45 (dd, ^3J = 7.62 Hz, ^4J = 1.63 Hz, 2H, H7), 7.22 (td, ^3J = 7.69 Hz, ^4J = 1.68 Hz, 2H, H5), 7.07 (td, ^3J = 7.52 Hz, ^4J = 0.98 Hz, 2H, H6), 6.81 (d, ^3J = 8.18 Hz, 2H, H4), 4.60 (s, 4H, H1). $^{13}C\{^1H\}$-RMN (100 MHz, $CDCl_3$, ppm) δ = 154.27 (C3), 131.0 (C7), 130.4 (C5), 129.7 (C2), 124.1 (C6), 118.6 (C4), –0.03 (C1).

Synthesis of the dialdehyde $S(C_6H_4CHO)_2$ (1b)

1b was prepared in a similar way as **1a** [29]. For the formation of the dilithiated compound, we used diphenylsulfide (5.0 mL, 30 mmol), dry hexane (40 mL), TMEDA (10.4 mL, 69.0 mmol), and *n*-butyllithium in hexanes (2.5 M, 36.1 mL, 90.2 mmol). Then, this mixture was refluxed for 40 minutes forming an orange

J. Mex. Chem. Soc. **2024**, *68*(2)
Regular Issue

ISSN-e 2594-0317

solution. The reaction was cooled down to 25 °C before dry DMF (8.1 mL, 105 mmol) was poured dropwise into the reaction mixture. The white solution was stirred for 1 h. Aqueous hydrochloric acid (30 mL HCl in 60 mL of distilled water) was added, and the mixture was stirred for fifteen minutes, followed by extraction with CH_3Cl (30 mL). The combined organic phases were dried (Na_2SO_4), and the volatiles were removed under reduced pressure to yield the **1b** as a brown viscous liquid (6.5 g, 90 %).

mw = 242.29 g/mol. IR (KBr, cm^{-1}): ν = 3059, 2850, 2738, 1688, 1584, 1458, 1440, 1259, 1198, 1040, 845, 822, 747. ^{1}H-RMN (400 MHz, $CDCl_3$, ppm) δ = 10.34 (s, 2H, H1), 7.95 (d, ^3J = 7.42 Hz, 2H, H7), 7.47 (m, 4H, H5), 7.16 (d, ^3J = 7.68 Hz, 2H, H6). $^{13}C\{^1H\}$-RMN (100 MHz, $CDCl_3$, ppm) δ = 191.7 (C1), 138.7 (C3), 135.1 (C2), 134.8 (C4), 132.7 (C7), 131.9 (C5), 128.0 (C6).

Synthesis of the diol $S(C_6H_4CH_2OH)_2$ (2b)

2b was prepared in a similar was as the **2a** compound. **1b** (6.5 g, 27 mmol), ethanol (40 mL), $Na[BH_4]$ (2.45 g, 64.8 mmol), diluted HCl (10 mL HCl in 20 mL of distilled water), CH_2Cl_2 (40 mL), brine (60 mL). The product was a yellow viscous liquid (6.6 g, 99 %).

mw = 246.32 g/mol. IR (KBr, cm^{-1}): ν = 3376, 3283, 3057, 2884, 1613, 1442, 1198, 1031, 747. ^{1}H-RMN (400 MHz, $CDCl_3$, ppm) δ = 7.45 (dd, ^3J = 7.50 Hz, ^4J = 0.82 Hz, 2H, H7), 7.27 (td, ^3J = 7.37 Hz, ^4J = 1.38 Hz, 2H, H6), 7.18 (td, ^3J = 7.30 Hz, ^4J = 1.54 Hz, 2H, H5), 7.12 (dd, ^3J = 7.73 Hz, ^4J = 1.28 Hz, 2H, H4), 4.72 (s, 4H, H1), 2.92 (s, 2H, O<u>H</u>). $^{13}C\{^1H\}$-RMN (100 MHz, $CDCl_3$, ppm) δ = 141.3 (C3), 133.3 (C2), 132.2 (C4), 128.8 (C7), 128.6 (C5), 127.9 (C6), 63.4 (C1).

Synthesis of the dichlorinated compound $[\{S(C_6H_4CH_2)_2\}Cl_2]$ (3b)

3b was prepared in a similar was as **3a**. **2b** (1.5 g, 6.2 mmol), carbon tetrachloride (20 mL), triphenylphosphine (3.6 g, 13.6 mmol). The yellow solution was chromatographed over a silica gel column with hexane/dichloromethane (1:1). The compound is a yellow liquid (0.77 g, 44 %).

mw = 267.14 g/mol. IR (KBr, cm^{-1}): ν = 3057, 2956, 2850, 1589, 1468, 1440, 1263, 1205, 1041, 821, 736, 666. ^{1}H-RMN (400 MHz, $CDCl_3$, ppm) δ = 7.51 (dd, ^3J = 7.50 Hz, ^4J = 1.10 Hz, 2H, H7), 7.30 (td, ^3J = 7.80 Hz, ^4J = 1.30 Hz, 2H, H6), 7.24 (td, ^3J = 7.40 Hz, ^4J = 1.30 Hz, 2H, H5), 7.16 (dd, ^3J = 7.71 Hz, ^4J = 0.90 Hz, 2H, H4), 4.79 (s, 4H, H1). $^{13}C\{^1H\}$-RMN (100 MHz, $CDCl_3$, ppm) δ = 138.2 (C3), 135.0 (C2), 132.9 (C4), 130.7 (C7), 129.7 (C5), 128.2 (C6), 44.5 (C1)

Synthesis of dibrominated compound $[\{S(C_6H_4CH_2)_2\}Br_2]$ (4b)

Dibrominated compound **4b** was synthesized according with the literature process [30]. To a toluene solution (20 mL) of diol **2b** (6.6 g, 26.79 mmol) was added dropwise HBr (10.8 mL, 93.76 mmol) dissolved in toluene (10 mL) and the resulting mixture was stirred for 22 h at reflux temperature. Then saturated aqueous $NaHCO_3$ solution (20 mL) was added carefully, followed by extraction with CH_3Cl (20 mL). The organic phase was separated, dried (Na_2SO_4) and evaporated to obtain a brown liquid. For the purification of the compound **4b**, a chromatographic column of the crude reaction is carried out, using silica as stationary phase and dichloromethane as eluent. From the purification a light-yellow viscous liquid was obtained, to crystallize the product were seeded crystals (2.5 g, 25 %).

mw = 372.11 g/mol. mp = 71 °C. IR (KBr, cm^{-1}): ν = 3051, 2973, 1563, 1469, 1440, 1218, 1038, 764, 730, 606. ^{1}H-RMN (400 MHz, $CDCl_3$, ppm) δ = 7.47 (dd, ^3J = 7.54 Hz, ^4J = 1.35 Hz, 2H, H7), 7.27 (td, ^3J = 7.07 Hz, ^4J = 1.55 Hz, 2H, H6), 7.22 (td, ^3J = 7.26 Hz, ^4J = 1.46 Hz, 2H, H5), 7.16 (dd, ^3J = 7.71 Hz, ^4J = 1.35 Hz, 2H, H4), 4.71 (s, 4H, H1). $^{13}C\{^1H\}$-RMN (100 MHz, $CDCl_3$, ppm) δ = 138.5 (C3), 135.2 (C2), 133.1 (C4), 131.2 (C7), 129.7 (C5), 128.2 (C6), 31.8 (C1).

Synthesis of diiodo compound $[\{S(C_6H_4CH_2)_2\}I_2]$ (5b)

Preparation of the title compounds was based on literature methods [31,32]. KI (1.12 g, 6.72 mmol) was added to **4b** (1.0 g, 2.69 mmol) dissolved in acetone (25 mL). This mixture was heated to reflux for 22 h. After the solvent was removed in vacuo, the residue was dispersed in CH_2Cl_2 (30 mL). The resulting precipitate was filtered off, and the solvent was removed in vacuo to yield the desired diiodo **5b** as a brown solid (1.23 g, 98 %).

mw = 466.10 g/mol. mp = 101 °C. IR (KBr, cm^{-1}): ν = 3043, 2929, 1557, 1470, 1437, 1206, 1151, 1030, 755. ^{1}H-RMN (400 MHz, $CDCl_3$, ppm) δ =7.45 (dd, ^3J = 7.56 Hz, ^4J = 1.51 Hz, 2H, H7), 7.22 (td, ^3J =

J. Mex. Chem. Soc. **2024**, *68*(2)
Regular Issue

ISSN-e 2594-0317

7.38 Hz, ^4J = 1.55 Hz, 2H, H6), 7.17 (td, ^3J = 7.49 Hz, ^4J = 1.56 Hz, 2H, H5), 7.11 (dd, ^3J = 7.70 Hz, ^4J =1.47 Hz, 2H, H4), 4.64 (s, 4H, H1). $^{13}C\{^1H\}$-RMN (100 MHz, $CDCl_3$, ppm) δ = 139.9 (C3), 134.3 (C2), 133.1 (C4), 130.7 (C7), 129.2 (C5), 128.3 (C6), 4.11 (C1).

Results and discussion

Synthesis

The overall linear synthesis of the respective diol compounds **Ch**$(C_6H_4CH_2$**OH**$)_2$ were based on a regioselective double-lithiation of the corresponding diphenyl(thio)ether, followed by a formylation reaction with DMF *in situ*; then a reduction of the resulting –CHO groups was carried out. Afterwards, the synthesis of the dichloro compounds **3a** and **3b** was carried out under Appel conditions, by using carbon tetrachloride and triphenylphosphine [33,34]. Dibrominated compounds **4a** and **4b** were obtained from a substitution reaction of the hydroxyl groups, by using Br^- as a nucleophile. Finally, the Br-by-I halide exchange to obtain **5a** and **5b** was achieved with an excess of potassium iodide in acetone, by using **4a** and **4b** as starting materials.

NMR analysis

NMR spectra of all compounds were recorded in $CDCl_3$ solutions at 25 °C; the assignment of the signals was carried out by the heteronuclear and homonuclear correlation of two-dimensional experiments (COSY, HSQC and HMBC). The signals of the aromatic protons of the ligand framework were observed as an ABCD pattern. In ^{13}C-NMR, six signals are observed for the different aromatic carbons; the signal found in higher frequency correspond to the carbons directly bonded to the heteroatom, due to the electron-withdrawing effect. This effect is more noticeable when **Ch** = O due to its higher electronegativity compared to the sulfur atom. On the other hand, the $–CH_2–$ signals for both series of compounds (**Ch** = O, S) were used to monitoring that the chemical transformations were successful. The changes of these signals are clearly noticeable on ^{13}C-NMR. Thus, when the carbon atom corresponds to the CHO functional group, the signal is around 190 ppm, and when the reduction reaction is carried out for its transformation into the $–CH_2–$OH group, the carbon signal shifts ca. 60 ppm low-frequency. Then, the carbon resonances for $–CH_2–$**X** were observed at 41.2, 28.2, 44.5, and 31.8 ppm for **3a**, **4a**, **3b**, and **4b**, respectively; when the halogen exchange occurs to obtain $–CH_2–$I, a considerable change in the displacement of these carbons towards frequencies close to 0 ppm was observed, this due to the electro-donating effect exerted by the iodine atom.

X-Ray single crystal analysis

Molecular structures of Ch$(C_6H_4CH_2X)_2$

There are some general features in the structural data of the **3a**–**5a** diphenylether and **4b** and **5b** diphenylthioether corresponding sets. In all compounds, the C_{sp2}–**Ch** and C_{sp3}–**X** bond distances are comparable to the covalent radii sum [$\Sigma r_{cov}(C_{sp2}, O)$ = 1.39 Å; $\Sigma r_{cov}(C_{sp2}, S)$ = 1.78 Å; $\Sigma r_{cov}(C_{sp3}, Cl)$ = 1.78 Å; $\Sigma r_{cov}(C_{sp3}, Br)$ = 1.96 Å; $\Sigma r_{cov}(C_{sp3}, I)$ = 2.15 Å][35]. Also, the C–**Ch**–C angles are practically equal in each set, being the C–O–C angle the wider one. The difference in C–**Ch**–C angles is the expected; this bond angle decreases as the atomic number of the chalcogen atom (**Ch**) increases, as has been discussed by Prof. Gillespie for several compounds of the ***p***-block, where the central atom has unshared lone pairs. [36] To analyze the conformations of the compounds in each set, we overlayed each pair of molecules (Figures 3 and 4). We used the Mercury 4.0 software [37] to calculate the root mean square deviation (RMSD) and the maximum deviation data in these superimpositions. Thus, we observed striking differences in the conformation of the diphenylether derivatives **3a**–**5a** in the solid state, despite the similitude of their skeletal structures. Firstly, the conformations of **3a** and **4a** are very similar (RMSD = 0.154 Å), regardless of their different crystalline systems and space groups (vide infra). The main conformational difference of this pair in comparison with **5a** lays on the direction of the C–**X** bonds; in **3a** (**X** = Cl) and **4a** (**X** = Br), the halogen atoms are pointed to opposite sides, while in the diiodo compound, the C–I bonds are oriented to the same side. For the diphenylthioethers **3b** and **4b**, the conformations are essentially the same (RMSD = 0.064 Å, with a maximum deviation of 0.154 Å, mainly due to the expected difference in C–**X** bond lengths). In these compounds, the halogen atoms are also pointed to opposite sides. We

J. Mex. Chem. Soc. **2024**, *68*(2)
Regular Issue

ISSN-e 2594-0317

also analyzed the C2–C3–**Ch**–C10 and C9–C10–**Ch**–C3 torsion angles. As a result, excepting the data for **5a**, the difference of these angles ($|\Delta_{ta}|$) is lesser than 10.3°, indicating a practically two-fold rotational symmetry (in fact, **4a** displays a perfect C_2 axis that bisects the C–O–C bond angle, with an obviously null difference in torsion angles). On the other hand, **5a** shows a difference of 76.7° that is consistent with an almost orthogonal arrangement of both phenyl rings around the C–O–C plane.

Crystal arrangement of Ch($C_6H_4CH_2X)_2$ derivatives

The chloro derivative **3a** crystallized in the triclinic system, while **4a** and **5a** pair crystallized in the monoclinic system, but in different space groups. On the other hand, both diphenylthioether compounds **4b** and **5b**, besides to be isostructural, they are also isomorphic, crystallizing in the centrosymmetric triclinic system, with a higher cell volume in **5b** due to the larger size of the iodine atoms. In all **Ch**($C_6H_4CH_2$**X**)$_2$ derivatives, notwithstanding the different nature of either **Ch** or **X** atoms, were observed non-classical C–H···**X** hydrogen bonding as well as p-interactions that contributes to the cohesion of the crystal (Fig. 5).

In the Fig. 5 we plotted a portion of the crystal structure where the molecules were related by their symmetry operators and, for the sake of comparison, we highlighted the C–H···**X** hydrogen bonding around the **X** atom in the asymmetric unit. In all plots, the asymmetric unit is displayed in gray color; the other colors are used for moieties related by other symmetry operation, such as inversion (in yellow) or, in the case of **4a**, rotation, rotation-inversion (both in green), and gliding (in magenta). The tagged distances of the intermolecular contacts and the symmetry operators for all compounds are summarized in Table 3. For **4a**, the asymmetric unit is just the half, with the oxygen atom positioned on a two-fold axis; the other half is generated by the corresponding two-fold rotation. As commented, **4b** and **5b** were isomorphic and, for conciseness, we just graph the structure of the iodo derivative. To build all the plots showed, we considered intermolecular H···**X** contacts smaller than 3.6 Å. From the plots, the number of contacts in the diphenylether derivatives decreases in the order **3a**>**4a**>**5a**; the magnitude of the distances must also decrease but in the inverse order because of the different atom sizes. On the other hand, the number of intermolecular interactions is the same in the diphenylthioethers **4b** and **5b**, as can be expected, because of their isomorphism.

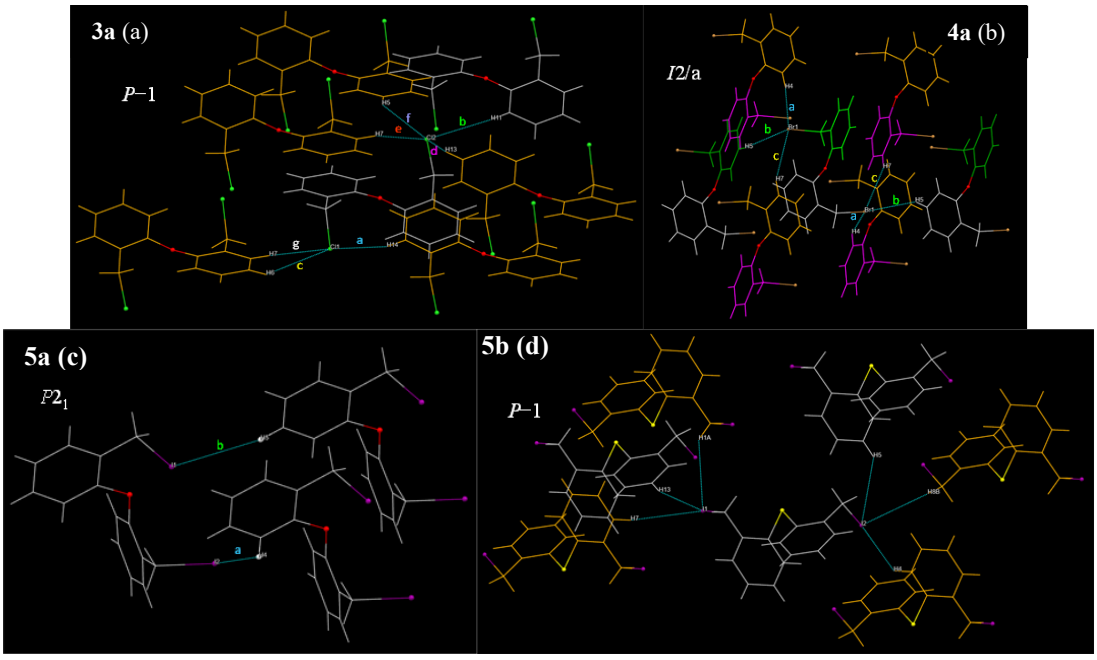

Fig. 5. C–H···**X** hydrogen bonding in **Ch**($C_6H_4CH_2$**X**)$_2$ derivatives (colours are used to highlight the symmetry operation involved in the generation of symmetry-related moieties; see text).

J. Mex. Chem. Soc. **2024**, *68*(2)
Regular Issue

ISSN-e 2594-0317

Table 3. Structural data of C–H···X hydrogen bonding in **Ch**($C_6H_4CH_2$**X**)$_2$ derivatives and symmetry operators.

tag	3a	4a	5a	4b	5b
a	2.918; C–H14···Cl1 1−x, 1−y, 1−z	3.047; C–H4···Br1 x, 1/2−y, −1/2+z	3.358; C–H4···I2 −1+x, y, z	3.160; C–H4···Br2 −1+x, y, z	3.239; C–H4···I2 1−x, 1−y, 1−z
b	3.106; C–H11···Cl2 −1+x, y, z	3.186; C–H5···Br1 −1/2+x, −1/2+y, −1/2+z	3.371; C–H5···I1 −1+x, 1+y, z	3.302; C–H13···Br1 x, y, −1+z	3.329; C–H13···I1 x, y, −1+z
c	3.108; C–H6···Cl1 2−x, 1−y, 2−z	3.207; C–H7···Br1 −1/2+x, 1−y, z	Not applicable	3.333; C–H5···Br2 x, y, −1+z	3.372; C–H5···I2 −1+x, y, z
d	3.130; C–H13···Cl2 1−x, −y, 1−z	Not applicable	Not applicable	3.374; C–H7···Br1 2−x, 2−y, −z	3.574; C–H7···I1 2−x, 2−y, −z
e	3.132; C–H7···Cl2 1−x, 1−y, 2−z	Not applicable	Not applicable	3.454; C–H8B···Br2 −x, 1−y, 1−z	3.582; C–H8B···I2 −x, 1−y, 1−z
f	3.181; C–H5···Cl2 1−x, −y, 2−z	Not applicable	Not applicable	3.469; C–H1A···Br1 1−x, 2−y, −z	3.499; C–H1A···I1 1−x, 2−y, −z
g	3.254; C–H7···Cl1 2−x, 1−y, 2−z	Not applicable	Not applicable	Not applicable	Not applicable

Hirshfeld surface analysis

The Hirshfeld surface (HS) encloses either a molecule or a cluster of molecules, and its corresponding 2D-fingerprint is unique for a given compound, therefore, the construction of this type of surfaces makes them a useful approach to compare crystal structures [23]. The surfaces based on the d_{norm} of all **Ch**($C_6H_4CH_2$**X**)$_2$ compounds clearly exhibit red spots in the vicinity of the **X** substituents, corresponding to the presence of close contacts due to C–H···**X** non-classical hydrogen bonding, i.e., contact distances that are shorter than the van der Waals radii sum [**3a**(1), **4a**(1), **5a**(1), **4b**(1), and **5b**(1) plots] in Fig. 6. The fragment patch plots are useful to calculate the number of molecules that interacts with a central one; also, the area data of these patches can be used to find the external major molecular fragments that are closer to a HS given. In Fig. 6 are plotted the corresponding fragment patches over the HS [**3a**(2), **4a**(2), **5a**(2), **4b**(2), and **5b**(2) plots]. In the O($C_6H_4CH_2$**X**)$_2$ compounds, the number of interacting molecules is 15, 20, and 16, for **3a**, **4a**, and **5a**, respectively (we considered a radius of 4.10 Å as an atom---atom distance, instead of the default value of 3.80 Å in CrystalExplorer). The four larger areas over the HS surface are 52.5, 43.0, 35.6, and 21.7 Å^2 for **3a** (52.5 % superficial area); 52.7, 51.6, 42.0, and 42.0 Å^2 for **4a** (63.0 % superficial area); and 63.6, 61.5, 29.9, and 20.3 Å^2 for **5a** (57.0 % superficial area). For the isomorphic **4b** and **5b** there are 16 molecules around the HS in each one; the larger areas are 52.5, 47.8, 44.5, and 44.1 Å^2 for **4b** (62.2 % superficial area); and 55.0, 48.4, 47.3, and 43.5 Å^2 for **5b** (61.7 % superficial area). Overall, four interacting molecules cover more than 52 % of each corresponding HS, despite their different surrounding number (see above).

J. Mex. Chem. Soc. **2024**, *68*(2)
Regular Issue

ISSN-e 2594-0317

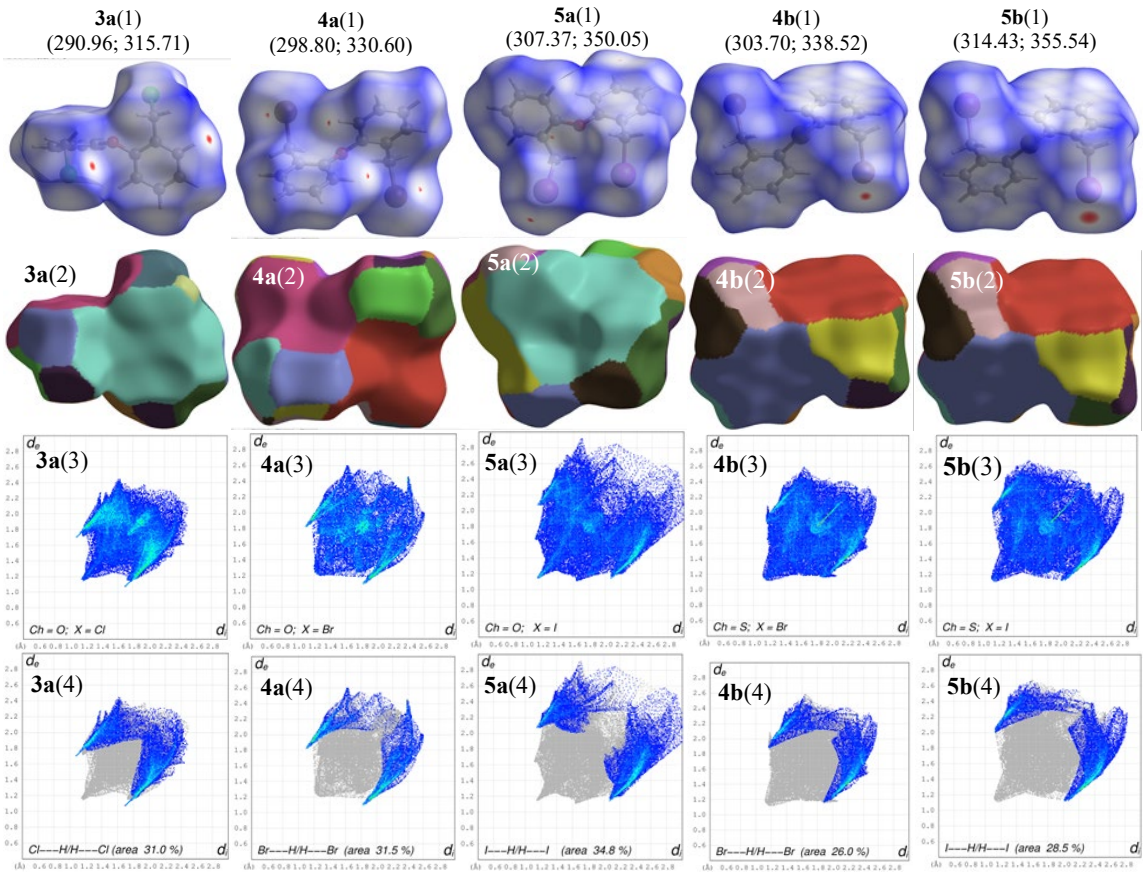

Fig. 6. Hirshfeld surfaces mapped over d_{norm}, fragment patches, and fingerprint plots for **Ch**($C_6H_4CH_2$**X**)$_2$ (**Ch** = O, S; **X** = Cl, Br, I) compounds (data in parentheses are superficial area in Å^2 and volume in Å^3).

To evaluate the contribution of the intermolecular contacts we plotted the 2D-fingerprints of the corresponding Hirshfeld surfaces [**3a**(3), **4a**(3), **5a**(3), **4b**(3), and **5b**(3) plots]. For the sake of comparison, we decomposed the corresponding overall 2D fingerprints plots in their **X**···H/H···**X** [**X** = Cl, Br, I; **3a**(4), **4a**(4), **5a**(4), **4b**(4), and **5b**(4) plots in Fig. 7] fingerprint plots for all compounds. We also plot the contribution of all contacts by means of a stacked bar chart, where we consider the reciprocal ones. The analysis of the intermolecular contact contributions for all compounds showed that H···H contacts are dominant, from 43.6 to 37.7 % contribution (Fig. 7). The next predominant non-covalent contributions are the **X**···H/H···**X** non-classic hydrogen bonding (green bars); we observed that compounds with **Ch** = O display higher values, probably due to the higher electronegativity of the oxygen atom in **3a**-**5a** when compared to the sulfur atom in **4b** and **5b**. To finish, the C···H/H···C (black bars) also display significant contributions due to the presence of the aromatic rings, which ones enhance C–H···pi as well as pi···pi interactions.

J. Mex. Chem. Soc. **2024**, *68*(2)
Regular Issue

ISSN-e 2594-0317

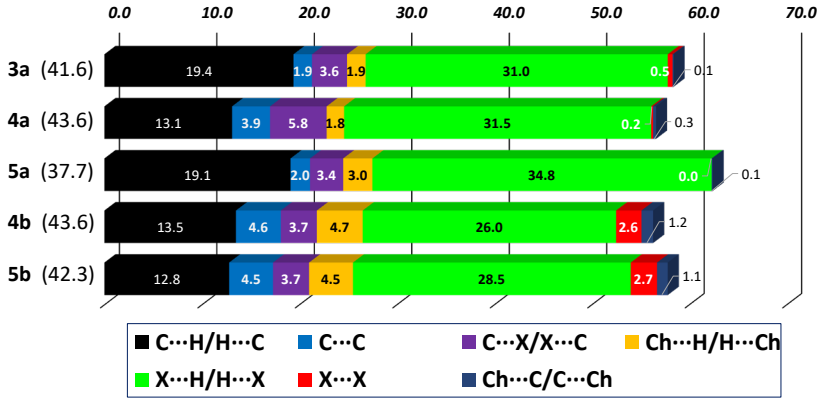

Fig. 7. Relative contributions in percentage of various intermolecular contacts of **Ch**($C_6H_4CH_2$**X**)$_2$ (**Ch** = O, S; **X** = Cl, Br, I) molecular crystals (H···H contacts are in parentheses).

A deeper analysis indicated that **4a** displayed a high C···Br/Br···C contribution (5.8 %, purple bar) in a centrosymmetric arrangement, and the isomorphic **4b**/**5b** pair displayed **X**···**X** notable contributions (red bars). In the first case, **4a** displayed C–Br···pi interactions alongside with other two C–H···Br interactions; the distance from this bromo atom to the centroid of the three C4, C5, and C6 aromatic atoms is 3.801 Å that is longer than the van der Waals radii sum [Σr_{vdW}(C, Br) = 3.55 Å]. The analysis of their Hirshfeld surfaces decorated with the molecular electrostatic potential (MEP) showed that the centrosymmetric arrangement of two molecules effectively displayed complementary interactions (see Fig. 8). The bromo atom in the C–Br bond display at its σ-hole position a positive potential (5.96 kcal/mol, in blue colour), while the three C(4), C(5), and C(6) aromatic atoms display a complementary negative potential (7.03 kcal/mol, in red colour) that is indicative of a C–Br···pi interaction of attractive nature. Something similar is observed for the C–H(4)···Br interaction, where the negative belt around the Br atom is displaying a negative potential (−15.06 kcal/mol, in red colour); as expected, the hydrogen atom in the C–H(4) bond has a positive potential (14.62 kcal/mol, in blue colour).

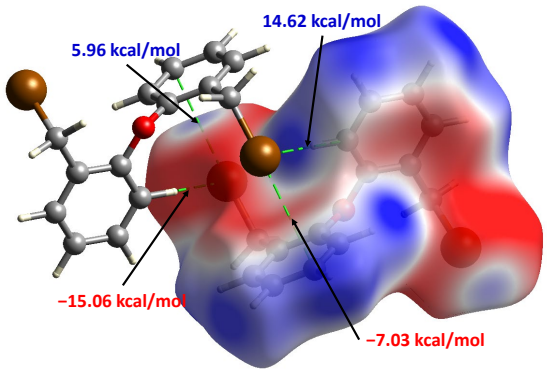

Fig. 8. Views of calculated electrostatic potential mapped on the Hirshfeld surface of **4a** showing the potential at the points of contact for Br···pi and C–H···Br noncovalent interactions.

Finally, as has been commented, the isomorphic **4b**/**5b** pair displayed **X**···**X** interactions (**X** = Br, I). In Fig. 9 we show the corresponding Hirshfeld surfaces decorated with the MEP to highlight just these interactions. In the front and rear plots, it is worth mentioning that there are differences in the positions of the head black arrow and the dashed lines that specify the shortest **X**···**X** interatomic distances intersecting the HS

J. Mex. Chem. Soc. **2024**, *68*(2)
Regular Issue

ISSN-e 2594-0317

decorated with the MEP. These positions are different because of we took the potential energy data from the intersection of the surface with the straight line coming from either outer or inner C–**X** bond, since in this position is where the s-hole is located. Each compound displays both complementary positive and negative potentials; the C–Br(1) and C–I(1) inner bonds display positive potentials of 7.53 and 11.61 kcal/mol for **4b** and **5b**, respectively (in blue color) while the matching negative potentials are −8.22 and −11.23 kcal/mol (in red color). Also, in the rear plots we show other positive potentials of 7.65 and 15.19 kcal/mol that match with the C(12) and C(13) benzenic carbons, similar to that observed in **4a**.

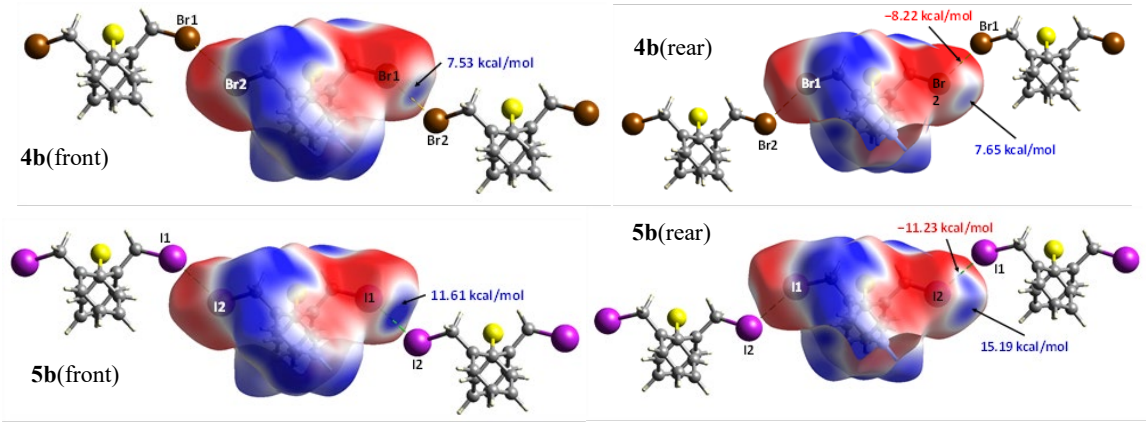

Fig. 9. Views of calculated electrostatic potential mapped on the Hirshfeld surface of **4b** and **5b** showing the potential at the points of contact for C–**X**···**X**–C (**X** = Br, I) noncovalent interactions.

Conclusions

Two series of dihalogenated compounds of general formula **Ch**($C_6H_4CH_2$**X**)$_2$ were synthetized by a linear approach from either cheap diphenylether or diphenylthioether used as starting materials. Despite the similitude in the skeletal structure, all compounds based on the ether framework displayed different interactions in the crystal arrangement. On the other hand, the thioether compounds were isostructural and isomorphic and, in these two cases we observed that the bromo- and iodo compounds were more susceptible to form **X**···**X** interactions and displayed little disposition to form **X**···H hydrogen bonding, due to the presence of the less electronegative sulfur atom as compared with the oxygen ones in the diphenylethers.

Acknowledgements

JVGG fully acknowledges the scholarship from CONACYT (ID 791450). This research was supported by project A1-S-12381 (CONACYT). CGGP acknowledges the financial assistant support from the same project (ID DIDI-DI- BECA-001).

References

1. Dean, J. A., in: *Lange's Handbook of Chemistry* (15th Edition), McGraw-Hill Education, New York, **1999**, 330.
2. Häggblom, M. M.; Bossert, I. D., in: *Halogenated Organic Compounds - A Global Perspective. In Dehalogenation.* Springer, Boston, MA, **2004**, 3-29. DOI: https://doi.org/10.1007/0-306-48011-5_1.

J. Mex. Chem. Soc. **2024**, *68*(2)
Regular Issue

ISSN-e 2594-0317

3. Patai S., Rappoport Z., in: *Halides, Pseudo-Halides and Azides*; *Part 1 and Part 2 in The Chemistry of Functional Groups*, John Wiley & Sons Ltd, **1983**, 1-223. DOI:10.1002/9780470771716.
4. Anderson B. M., Meyers R. A.; in: *Halogen Chemistry*. *In Encyclopedia of Physical Science and Technology* (Third Edition), Academic Press, Elsevier, **2003**, 197-222. DOI: https://doi.org/10.1016/B0-12-227410-5/00307-0.
5. Smolnikov, S.; Bin Shahari, M.; Dolzhenko, in: *Green sustainable process for chemical and environmental engineering and science: A. Sonochemical protocols for Grignard reactions*. Elsevier, **2020**, 243-255. DOI: 10.1016/B978-0-12-819540-6.00009-7.
6. Odd Hassel – Nobel Lecture. NobelPrize.org. Nobel Prize Outreach AB 2023. Sun. 19 Mar 2023. https://www.nobelprize.org/prizes/chemistry/1969/hassel/lecture/
7. Desiraju, G. R.; Ho, P. S.; Kloo, L. Legon, A. C.; Marquardt, R.; Metrangolo, P.; Politzer, P.; Resnati, G.; Rissanen, K. *Pure Appl. Chem.* **2013**, *85*, 1711–1713. DOI: http://dx.doi.org/10.1351/PAC-REC-12-05-10.
8. Cavallo, G.; Metrangolo, P.; Milani, R.: Pilati, T.; Priimagi, A.; Resnati, G. Terraneo, G. *Chem. Rev.* **2016**, *116*, 2478-2601. DOI: https://pubs.acs.org/doi/10.1021/acs.chemrev.5b00484.
9. Metrangolo, P.; Neukirch, H. Pilati, T.; Resnati, G. *J. Am. Chem. Soc.* **2005**, *38*, 386–395. DOI: https://doi.org/10.1021/ar0400995.
10. Sutar, R. L.; Huber, S. M. *J. Am. Chem. Soc.* **2019**, *9*, 9622–9639. DOI: https://doi.org/10.1021/acscatal.9b02894.
11. Ding, X., Tuikka, M.; Haukka, M., in: *Halogen Bonding in Crystal Engineering: Recent Advances in Crystallography*, IntechOpen, **2012**, 143-168. DOI: https://doi.org/10.5772/48592.
12. Nunzi, F.; Cesario, D.; Tarantelli, F.; Belpassi, L. *Chem. Phys. Lett*. **2021**, *771*, 138522. DOI: https://doi.org/10.1016/j.cplett.2021.138522.
13. Prasanna, M.D.; Guru Row, T.N. *Cryst. Eng.* **2000**, *3*, 135-154. DOI: https://doi.org/10.1016/S1463-0184(00)00035-6.
14. Zhao-Qi, G.; Shi-Hui, Q.; Huan-Hui, Y.; Shan-Chao, W.; Meng, Z.; Gui-Mei, T.; Yong-Tao, W.; Tao, A.; Seik-Weng N. *J. Mol. Struct.* **2022**, *1267*, 133606. DOI: https://doi.org/10.1016/j.molstruc.2022.133606.
15. Mejia-Rivera, F. J.; Alvarado-Rodríguez, J. G.; Andrade-López, N.; Cruz-Borbolla, J.; Jancik, V. *Inorg. Chem. Commun.* **2018**, *97*, 44-48. DOI: https://doi.org/10.1016/j.inoche.2018.09.006.
16. Nather, C.; Jess, I.; Kus, P.; Jones, P.G. *Cryst. Eng. Comm.* **2016**, *18*, 3142
17. Xu, X.; Strongin, R.M.; Fronczek, F.R. *CSD Communication (Private Communication),* **2015**.
18. Oxford Diffraction CrysAlis software system, version 1.171.37.35. Oxford Diffraction Ltd., Abingdon, UK (**2014**)
19. Dolomanov, O.V.; Bourhis, L.J.; Gildea, R.J.; Howard, J.A.K.; Puschmann H. J. *Appl. Cryst.* **2009**, *42*, 339–341.
20. Sheldrick, G.M. *Acta Cryst. A.* **2015***, 71*, 3–8.
21. Sheldrick, G.M. *Acta Cryst. C.* **2015**, *71*, 3–8.
22. Spackman, M.A.; Jayatilaka, D. *CrystEngComm*. **2009**, *11*, 19–32
23. Spackman, P.R.; Turner, M.J.; McKinnon, J.J.; Wolff, S.K.; Grimwood, D.J.; Jayatilaka, D.; Spackman, M.A. *J. Appl. Cryst.* **2021**, *54*,1006–1011.
24. Jayatilaka, D.; Grimwood D.J. *Comput. Sci. ICCS*, **2003**, *4*, 142–151.
25. Becke A.D. *J. Chem. Phys.* **1993**, *98*, 5648–5652
26. Godbout, N.; Salahub, D. R.; Andzelm J.; Wimmer Can, E. *J. Chem.* **1992**, *70*, 560–571.
27. Sosa, C.; Andzelm, J.; Elkin, B.C.; Wimmer, E.; Dobbs, K.D.; Dixon D.A. *J. Phys. Chem.* **1992**, *96*, 6630–6636.
28. Osuka, A.; Kobayashi, F.; Maruyama, K. *Bull. Chem. Soc. Jpn.* **1991***, 64*, 1213-1225. DOI: https://doi.org/10.1246/bcsj.64.1213.

J. Mex. Chem. Soc. **2024**, *68*(2)
Regular Issue

ISSN-e 2594-0317

29. Britovsek, G. J. P.; Gibson, V. C.; Hoarau, O. D.; Spitzmesser, S. K.; White, A. J. P.; Williams, D. J. *Inorg. Chem.* **2003**, *42*, 3454-3465. DOI: https://doi.org/10.1021/ic034040.
30. Martínez-Otero, D.; Alvarado-Rodríguez, J. G.; Cruz-Borbolla, J.; Andrade-López, N.; Pandiyan, T.; Moreno-Esparza, R.; Flores-Alamo, M.; Cantillo-Castillo J. *Polyhedron.* **2012**, *33*, 367-377. DOI: https://doi.org/10.1016/j.poly.2011.11.053.
31. Kida, T.; Kikuzawa, A.; Higashimoto, H.; Nakatsuji, Y.; Akashi, M. *Tetrahedron*. **2005**, *61*, 5763–5768. DOI: https://doi.org/10.1016/j.tet.2005.04.026.
32. McAdam, C.J.; Hanton, L.R.; Moratti, S.C.; Simpson*, J. Acta Crystallogr. E: Crystallogr. Commun*. **2015**, *71*, 1505-1509. DOI: 10.1107/S2056989015021295.
33. Appel, R. *Angew. Chem. Int. Ed. Engl.* **1975**, *14*, 801-811. DOI: https://doi.org/10.1002/anie.197508011.
34. Cristol, S. J.; Strom, R. M.; Stull, D. P., *J. Org. Chem*. **1978**, *43*, 1150. DOI: https://doi.org/10.1021/jo00400a027.
35. Cordero, B.; Gómez, V.; Platero-Prats, A. E.; Revés, M.; J. Echeverría, J., Cremades, E.; Barragán F.; Alvarez, S. *Dalton Trans*. **2008**, *21*, 2832-2838. DOI: https://doi.org/10.1039/B801115J.
36. Gillespie, R.J. Popelier, P.L.A., in: *Chemical Bonding and Molecular Geometry; From Lewis to Electron densities.* Oxford University Press, New York, **2001**, 84. DOI: 10.1021/ed080p31.
37. Macrae, C. F.; Sovago, I.; Cottrell, S. J.; Galek, P. T. A.; McCabe, P.; Pidcock, E.; Platings, M.; Shields, G. P.; Stevens, J. S.; Towler, M.; Wood, P. A. *J. Appl. Cryst.* **2020**, 53, 226-236. DOI: https://scripts.iucr.org/cgi-bin/paper?gj5232.